Geometrical optical analysis of gradient refractive index microresonator

TIANCI CHEN, ZHAOFENG KANG, YU YANG, SHUAI ZHAO, JUN ZHANG, LEI ZHANG, AND KEYI WANG*

Department of Precision Machinery and Precision Instrumentation, University of Science and Technology of China, Hefei 230026, China
*kywang@ustc.edu.cn

Abstract: Optical microresonators confine light to small volumes through resonant circulation. Herein, the whispering gallery mode (WGM) microresonators have high *Q* factors among these microresonators, which have significant research value in the fields of fundamental physics research and optoelectronic devices. However, maintaining a very high surface finish on the side of the microresonator is necessary, and keeping a coupling distance of tens of nanometers between the microresonator and the coupling waveguide. Thus, this makes the fabrication, coupling, and packaging of the microresonator very difficult, and seriously hinders the practical application of the microresonator. In this study, the concept of gradient refractive index (GRIN) microresonator is proposed, and the radial GRIN is introduced to change the light direction and form a closed optical path within the microresonator. Herein, the mode field position of the GRIN microresonator is derived from the light transmission equation, and the theoretical result is proved by FDTD simulation. Hence, there are several advantages to using this novel optical microresonator, including its high *Q* factor, strong coupling stability, and ease of integration.

1. Introduction

WGM microresonator confines light to small volumes with high *Q* factor through resonant circulation [1-2]. It has been widely researched for over two decades, being used in sensors [3], narrow linewidth lasers [4], and nonlinear optics [5]. In the WGM microresonators, light is continuously reflected on the inside surface as a result of the significant difference in refractive index between the cavity and the surrounding environment [6]. The mode is confined near the surface at the equator, and part of the energy is exposed to the environment in the form of an evanescent field [7]. Moreover, WGM microresonators are susceptible to surface finish and environmental pollution and have the disadvantages of limited *Q* factors, poor coupling stability, and a difficult package [8-12]. Therefore, we consider using a brand-new type of microresonator that is independent of surface reflection and whose mode field is below the surface to replace the WGM microresonators.

In addition to surface total internal reflections, gradient refractive index (GRIN) can also change the direction of light propagation. Self-focusing lenses can be produced by GRIN in the radial direction of glass rods, which have been widely used in optical fiber couplers, semiconductor laser collimators, and so on, and have a wide range of applications in the optical communication field [13]. Earlier articles have discussed the characteristics of WGM microresonators manufactured with GRIN medium [14-18]. In 2003, V. S. Ilchenko et al. discovered that if GRIN material is used for WGM microcavity, the position of the mode field will be shifted inward, thus significantly increasing the *Q* factor [14]. Meanwhile, in 2012, Di Zhu et al. proposed the use of GRIN cladding to make light more easily coupled into the liquid core cylindrical WGM cavity [15]. Moreover, in 2014, K. Dadashi et al. showed solutions of the Helmholtz equation for a 2D Maxwell's fish eye WGM microresonator [16]. Furthermore, in 2016, Z. Najafi et.al. studied WGM microdisk resonator sensors with GRIN to achieve higher

sensitivity [17]. Meanwhile, based on [14], S. Balac et al. studied WGMs in GRIN microdisk resonators using a quantum mechanical analogy in 2020 [18].

Although GRIN microresonators with various refractive index distributions have been studied, an explanation of the geometrical optical nature of GRIN microresonators is still lacking. In this paper, we analyze the GRIN microresonator with geometric optics, which is completely different from the WGM microresonator. This is because only the refractive index gradient and curvature are used to alter the direction of the light ray. There is no reflection, thus, there is no surface scattering. Hence, it is reasonable that GRIN microresonators have the advantages of a high Q factor, pure fundamental mode, robust coupling stability, and ease of integration.

In Section 2, the fundamental mode position and high-order mode characteristics are calculated and derived from the light ray equation, and we explain the reason for the high Q of GRIN microresonators. Meanwhile, in Section 3, FDTD is used to simulate GRIN microresonators with constant coefficient ion diffusion to prove the conclusion.

2. Geometrical optical analysis of GRIN microresonators

2.1 The fundamental mode position

GRIN microresonators have an axisymmetric radial refractive index distribution. Herein, the GRIN microresonator confines the light field inside the microresonator by continuously changing the refractive index gradient near the edge as compared to the WGM microresonator which uses surface total internal reflections. In the GRIN medium, the light path is controlled by the light ray equation. The light can be transmitted along the closed-loop circle by designing the radial refractive index gradient in the cylinder, that is, the light can be constrained by the refractive index gradient to form a closed circular waveguide in the microresonator. In addition, the evanescent field and leak mode can be coupled with the waveguide or prism by properly grinding and polishing to the position near the circular waveguide. In the GRIN microresonator, the transmitted light is confined within the medium.

Considering any light ray S and integrating the refractive index n of any segment of its starting point s_0 and ending point s, the optical path can be obtained

$$L = \int_{s_0}^{s} n\mathrm{d}s. \tag{1}$$

Due to the characteristics of the GRIN process, the GRIN microresonator has spherical symmetry or cylindrical symmetry. We consider the case of spherical symmetry (since the result is polar mode field position, it also applies to cylindrical symmetry): $n = f(r)$, where $r = (x^2 + y^2 + z^2)^{1/2}$.

Because of Fermat's principle, the path of light propagation is the path with the extreme value of the optical path, it conforms to Euler's equation $(nr')' = \nabla n,$ or

$$nr'' + n'r' = \dot{n}\frac{\boldsymbol{r}}{r}, \tag{2}$$

where a prime indicates d/ds, and a dot indicates d/dr.

According to Fig. 1, the optical path relationship is transformed from the differential of s to that of r, as follows,

$$\mathrm{d}s = \sqrt{\mathrm{d}r^2 + (r\mathrm{d}\theta)^2} = (1 + r^2\dot{\theta})^{1/2}\,\mathrm{d}r, \tag{3a}$$

$$\sin\psi = r\theta' = r\frac{\mathrm{d}\theta}{\mathrm{d}s} = r\frac{\dot{\theta}}{\dot{s}} = r\left|\dot{\theta}\right|(1 + r^2\dot{\theta})^{-1/2}, \tag{3b}$$

where ψ is defined as the angle between the tangent and the radius vector from the origin.

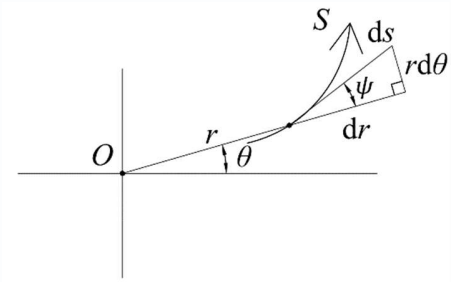

Fig. 1 Parameter interpretation of optical propagation.

Eq. (1) takes the form

$$L = \int_{r_0}^{r} n(r)(1 + r^2\dot{\theta})^{1/2}\,\mathrm{d}r. \tag{4}$$

Regarding r as an independent variable, the Euler equation gives

$$\frac{\partial F}{\partial \theta} - \frac{\mathrm{d}}{\mathrm{d}r}\left(\frac{\partial F}{\partial \dot{\theta}}\right) = 0, \tag{5a}$$

that is,

$$\frac{\mathrm{d}}{\mathrm{d}r}[nr^2\dot{\theta}(1 + r^2\dot{\theta})^{-1/2}] = 0, \tag{5b}$$

We can get invariant e, which has the same sign as $\dot{\theta}$.

$$e = nr^2\dot{\theta}(1 + r^2\dot{\theta})^{-1/2} = \pm nr\sin\psi, \tag{6}$$

By logarithmic differentiation of Eq. (6) we have

$$\frac{n'}{n} + \frac{r'}{r} + \frac{\psi'}{\tan\psi} = 0, \tag{7}$$

simplified as

$$\psi' = -\theta'\left(1 + \frac{rn'}{nr'}\right). \tag{8}$$

The slope angle at any point of the curve is $\psi + \theta$ as seen in Fig. 1, so the curvature

$$K = \psi' + \theta' = -\frac{rn'\theta'}{nr'} = -r\theta'\frac{\dot{n}}{n}. \tag{9}$$

The above is the classical calculation method of geometrical optics. Next, we consider the GRIN microresonator. As the fundamental mode of the GRIN microresonator, the light always circulates on a circle with a fixed radius (as shown in Fig. 2), resulting in

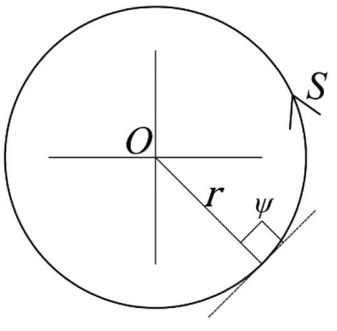

Fig. 2 Fundamental mode of the GRIN microresonator.

$$K = \frac{1}{r}, \tag{10a}$$

And

$$\psi = 90°. \tag{10b}$$

Then we can get

$$\sin\psi = r\theta' = 1, \tag{11a}$$

And

$$e = nr\sin\psi = nr, \tag{11b}$$

In combination with Eq. (9), (10a), and (11a), it can be obtained

$$-\dot{n} = \frac{n}{r}. \tag{12}$$

As shown in Fig. 3, The outer ring with radius R is the edge of the resonator and the inner ring with radius r_0 is the calculated fundamental mode position from Eq. (12). For any GRIN microresonator, if two curves, -dn/dr and n/r, are generated, their intersection point describes the fundamental mode position. In addition, considering

$$\frac{\mathrm{d}(nr)}{\mathrm{d}r} = n + \dot{n}r = 0. \tag{13}$$

for any radial distribution of refractive index, if the $n(r)r$ curve is made, the pole of the curve is the fundamental mode position, just the same as Eq. (12).

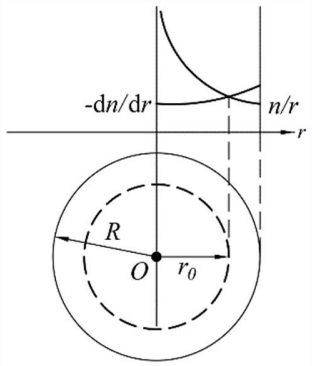

Fig. 3 The intersection point of -dn/dr and n/r describes the fundamental mode position of the GRIN microresonator.

2.2. The characteristics of the high-order mode

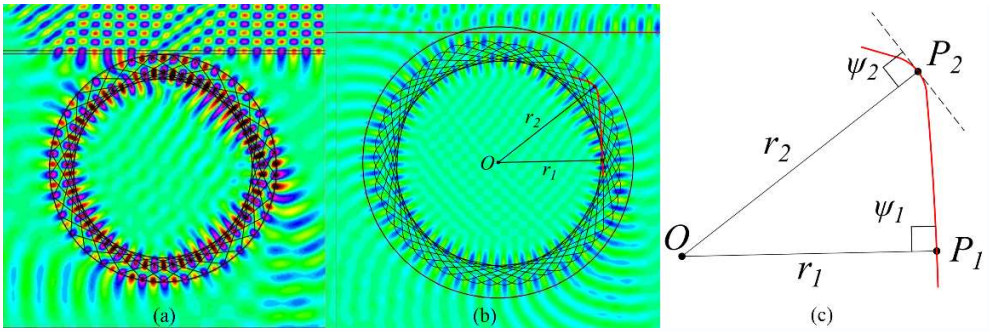

Fig. 4 (a) High-order mode of the WGM microresonator. (b) High-order mode of the GRIN microresonator. (c) Description of highlighted light in b.

The high-order mode of WGM can be conceived as the interference result of light reflecting at the interface repeatedly to form a closed optical path, as shown in Fig. 4(a). There is no interface reflection found in the GRIN microcavity, only light bending caused by curvature and refractive index gradient. Its high-order mode can be conceived as the interference result of the light bending near the edge repeatedly to form a closed optical path, as shown in Fig. 4(b). Meanwhile, the outer ring mode field is the location of the light bounce point with radius r_2 and the inner radius of the interfering ring is r_1. A small portion of the highlighted light is shown in Fig. 4(c). The light propagates from the nearest point P_1 of the center of the microcavity to the farthest point P_2 and then is bent back into the cavity. Both two points have

$$\psi_1 = \psi_2 = 90°, \tag{14}$$

where ψ is defined as the angle between the tangent and the radius vector from the origin.

Considering the well-known invariant $e=\pm nr\sin\psi$ from Eq. (6), the sign of e is the same in the same direction of ray, so $n(r)r$ of the nearest point and the farthest point of the high-order mode are equal

$$e = n_1 r_1 = n_2 r_2. \tag{15}$$

That's the high-order mode characteristic of the GRIN microresonator.

2.3. Qualitative analysis of GRIN microresonators

There is no total reflection at the interface of the GRIN microresonators, and it is not affected by surface roughness, environment, surface pollution, surface adsorption, and other factors. Hence, its optical performance is stable, thus, it can be expected that the Q factor of the GRIN microresonator is much higher than that of the WGM microresonator.

When the optical power circulating inside the resonator is below the threshold of nonlinear effects, the Q factor of the resonator coupling system is mainly composed of four parts [19]

$$\frac{1}{Q} = \frac{1}{Q_{\text{mat}}} + \frac{1}{Q_{\text{ss}}} + \frac{1}{Q_{\text{rad}}} + \frac{1}{Q_{\text{ex}}} \tag{16}$$

Material loss $Q_{\text{mat}} = \dfrac{2\pi n}{\alpha\lambda}$ is the optical loss of microresonator materials, where α is the absorption coefficient. The Q factor of the GRIN microresonator is dominated by materials absorption and will have a Q factor of $>10^{11}$ that approaches the absorption limit of the material [20].

Scattering Q_{ss} is significant for WGM microresonators because of the large variation in refractive index caused by surface roughness. In contrast, when processes such as ion diffusion are used, the scattering loss is minimal for GRIN microresonators given that the refractive index perturbation on the mode field position is substantially reduced.

Meanwhile, the third is radiation loss $Q_{\text{rad.}}$ Based on the simulations in Section 3, it is effective to minimize radiation loss by preventing the mode field from extending beyond the edge of the microresonator by controlling the refractive index distribution. Herein, the radiation loss of the GRIN microresonator is negligible with a radius higher than 15 μm, similar to that of the WGM microresonator [21].

The above three factors belong to the intrinsic Q factors and there is also an external coupling Q_{ex} of the whole system. In general, the coupling between WGM microresonators and waveguides requires air gaps, thus, the high index contrast forms a potential barrier causing loss [21]. However, GRIN microresonator and waveguide can be directly bonded and can be regarded as waveguide-to-waveguide coupling. The small index contrast leads to low coupling loss. Meanwhile, the GRIN microresonator can maintain a more stable coupling structure by directly bonding with waveguides or prisms.

3. Simulation of the fundamental mode of the GRIN microresonator

3.1 The simplest GRIN microresonator with the ion exchange process

GRIN optical materials have been widely used in the field of self-focusing lenses and optical fibers. There are various fabrication processes, such as the ion exchange process, vapor deposition process, neutron irradiation process, polymer polymerization process, ion-filling process, crystal growth process, a vacuum evaporation process, sol-gel process, and silicon thermal oxidation process [22]. This paper analyzes the optical characteristics of GRIN microresonators using the ion exchange process as an example.

In the ion exchange process, the host material is heated and immersed in molten salt, where ions (usually monovalent cations) in the molten salt replace different ions in the host material and maintain electrical neutrality. Herein, there are two steps: one is the ion exchange whereby two kinds of ions exchange each other at the interface between the host material and molten salt; the other is the diffusion and migration of the ions entering the surface of the host material to the interior, while the diffusion and migration of the replaced ions in the interior to the surface.

Ion diffusion is defined as a mass transfer process caused by thermal motion. During this process, ion concentration varies with location and time. The ion diffusion in the cylindrical host material satisfies Fick's second law of diffusion:

$$\frac{\partial u}{\partial t} = \frac{1}{r}\frac{\partial}{\partial t}[r \cdot D(u)]\frac{\partial u}{\partial r}. \tag{17}$$

Its initial conditions and boundary conditions can be written as follows:

$$u(1,t) = 0, \tag{18a}$$

$$u(r,0) = 1, \tag{18b}$$

where r is the normalized radius, u (r, t) is the normalized concentration, $u = \frac{c - c_1}{c_0 - c_1}$, c_1 is the concentration at exchange equilibrium, and c_0 is the original concentration.

Assuming that the mutual diffusion coefficient D is constant D_0, there is an analytical solution:

$$u(r,\tau) = 2\sum_{n=1}^{\infty} \exp(-\alpha_n \tau)\frac{J_0(r\alpha_n)}{\alpha_n J_1(\alpha_n)}, \tag{19}$$

where α_n is the root of the zero-order Bessel function, J_0 and J_1 are zero-order and first-order Bessel functions, respectively, $\tau = \frac{Dt}{R^2}$ is dimensionless diffusion time, and R is the actual radius of the cylinder.

Simulations based on the refractive index distribution generated by constant-coefficient diffusion will be carried out in this paper. The relationship between the fundamental mode field position and diffusion time is depicted in Fig. 5(a) by replacing the thallium-containing glass, which has a radius of 75 μm and a refractive index of 1.64, with sodium ions. As the diffusion time increases, the fundamental mode field position moves inward initially and then outward. Therefore, there is always an ideal diffusion time for any pair of ion exchange materials. Thus, controlling the dimensionless diffusion time to 0.0004, the radial refractive index distribution $n(r)$ is shown in the black line in Fig. 5(b). Herein, the curve of $n(r)r$ was obtained as shown in the red line, and its poles were calculated to obtain the fundamental mode position of 72.55 μm. The distance from the surface is 2.45 μm, which can ensure that the mode field is completely located within the microresonator.

Several commonly used GRIN materials are selected to calculate the fundamental mode field position near the ideal diffusion time by Eq. (13), as shown in Table. 1. Herein, as long as the radius of the cavity is larger than 100 μm, the center of the mode field can be moved to several microns within the cylinder edge by the ion exchange process, and the GRIN microresonator can be formed.

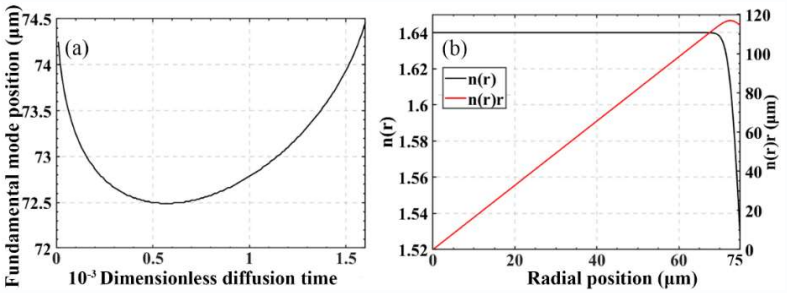

Fig. 5 Thallium-containing glass with constant coefficient diffusion. (a) The relationship between the fundamental mode field position and diffusion time. (b) *n(r)* and *n(r)r* curve with dimensionless diffusion time of 0.0004.

Table.1 Fundamental mode field position of several ion exchange pairs near the ideal diffusion time

Host material	Refractive index	Ion exchange pair	Index difference	Dimensionless diffusion time	Radius	Fundamental mode field position
$LiNbO_3$	2.211	Li^+-K^+	-0.109	0.0003	25 μm	24.40 μm
					100 μm	97.60 μm
					500 μm	488.10 μm
					1 mm	976.15 μm
BaF_2	1.466	Ba^{2+}-Mg^{2+}	-0.095	0.0005	25 μm	24.20 μm
					100 μm	96.85 μm
					500 μm	484.30 μm
					1 mm	968.65 μm
Thallium-containing glass	1.640	Tl^+-Na^+	-0.114	0.0004	25 μm	24.20 μm
					100 μm	96.75 μm
					500 μm	483.70 μm
					1 mm	967.35 μm

3.2 FDTD Simulation of the fundamental mode of GRIN microresonator with constant coefficient diffusion

The 75 μm radius GRIN microresonator from the previous subsection is simulated using the FDTD program. First, the Gaussian pulse wave with a center wavelength of 1550 nm is coupled into the resonator at a 70° angle through a prism with a refractive index of 1.73. In addition, with the ambient refractive index of 1, the FFT diagram displaying both the GRIN mode and WGM is shown in Fig. 6(a). On this basis, the ambient refractive index is set to 1.526 to entirely rule out the effect of WGM, which is the same as the refractive index of the edge of the GRIN resonator. The FFT result of sampling at the predicted fundamental mode position is shown in Fig. 6(b), thereby demonstrating its superior single-mode characteristics. A monochromatic light with a resonant wavelength of 1552.57 nm is coupled into the GRIN microresonator, as shown in Fig. 6(c). The outer ring is the edge of the resonator, and the inner ring is the position of the prediction mode field. The entire mode field is located within the cavity, and the center of the mode field is located at the predicted position. Considering that the radius is relatively large, the mode field width is relatively small. The enlarged view of the bottom of the resonator in Fig. 6(d) shows the pure single-mode feature.

Furthermore, the same method is used to simulate resonators with the same dimensionless diffusion time but different radii. The simulated fundamental mode positions of the GRIN microresonators of thallium-containing glass with different radii are shown as red dots in Fig. 6 (e), and the R-square value of the theoretical derived position (black dashed line) is 0.99993, which indicates that the fundamental mode positions of the GRIN microresonators derived are accurate.

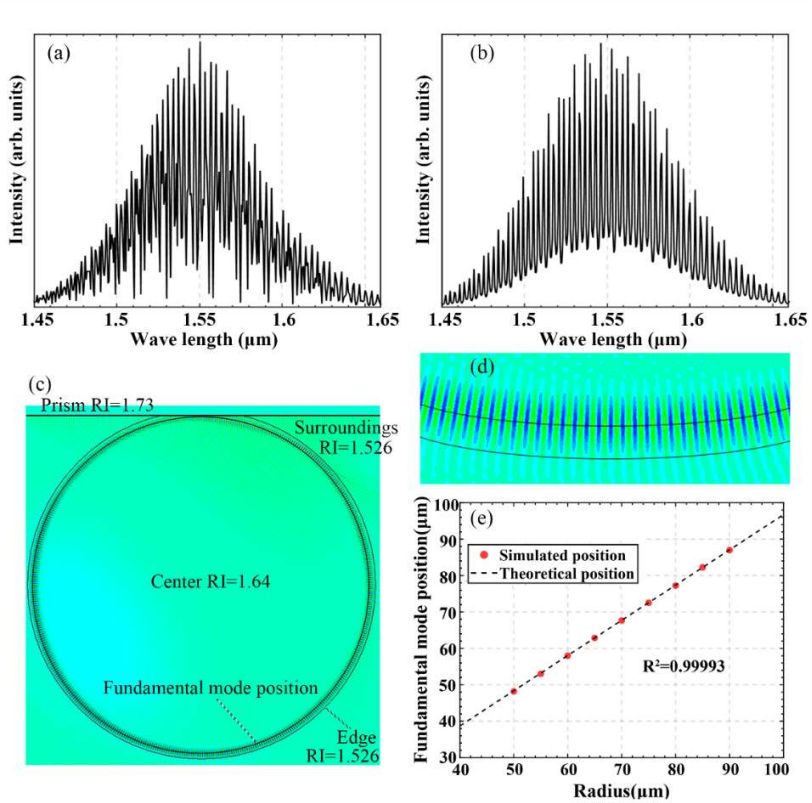

Fig. 6 FDTD Simulation of thallium-containing glass. (a) FFT with the ambient refractive index of 1. (b) FFT with the ambient refractive index of 1.526. (c) FDTD simulation of b. (d) enlarged view of the bottom of c. (e) Fundamental mode positions of resonators with different radii.

4. Summary

GRIN microresonator expands a new system of gradient index optics and establishes a new field of optical microcavities. It has broad application prospects because of its high Q factor, pure fundamental mode, robust coupling stability, and ease of integration.

Hence, this paper proposes the GRIN microresonator as a novel optical microresonator. The entire light field is contained inside the resonator using the continuously varying gradient of refractive index near the edge of the resonator. In addition, the GRIN microresonator has a higher Q factor, a more robust coupling structure, and a more integrated package than the WGM microresonator. The ray equation is used to determine the fundamental mode's position and the high-order mode's characteristics. The fundamental mode's location on the $n(r)r$ curve is at the pole. Moreover, the high-order mode light's $n(r)r$ is the same at both its closest and farthest points. Furthermore, the GRIN microresonators with the ion exchange process are verified by the FDTD simulation.

Disclosures. The authors declare that there are no conflicts of interest related to this article.

Data availability. Data underlying the results presented in this paper are not publicly available at this time but may be obtained from the authors upon reasonable request.

Reference

[1] K. Vahala. “Optical microcavities.” Nature 424.6950: 839-846 (2003).

[2] W. Wang, L. Wang, and W. Zhang. “Advances in soliton microcomb generation.” Advanced Photonics 2.3: 034001 (2020).

[3] T. Lu, H. Lee, T. Chen, S. Herchak, J. H. Kim, S. E. Fraser, R. C. Flagan, and K. Vahala. “High sensitivity nanoparticle detection using optical microcavities.” Proceedings of the National Academy of Sciences, 108(15), 5976-5979 (2011).

[4] W. Liang, V. S. Ilchenko, D. Eliyahu, A. A. Savchenkov, A.B. Matsko, D. Seidel, and L. Malek. “Ultralow noise miniature external cavity semiconductor laser.” Nature communications 6.1: 1-6 (2015).

[5] T. J. Kippenberg, R. Holzwarth, and S. A. Diddams. “Microresonator-based optical frequency combs.” Science 332.6029: 555-559 (2011).

[6] C. G. B. Garrett, W. Kaiser, and W. L. Bond. “Stimulated emission into optical whispering modes of spheres.” Physical Review 124.6: 1807 (1961).

[7] V. B. Braginsky, M. L. Gorodetsky, and V. S. Ilchenko. “Quality-factor and nonlinear properties of optical whispering-gallery modes.” Physics letters A 137.7-8: 393-397 (1989).

[8] Y. Yan, C. ZHOU, and J. Xiong. “Packaged silica microsphere-taper coupling system for robust thermal sensing application.” Optics express 19.7: 5753-5759 (2011).

[9] Y. Dong, K. Wang, and X. Jin. “Packaged microsphere-taper coupling system with a high Q factor.” Applied optics 54.2: 277-284 (2015).

[10] M. L. Gorodetsky, A. A. Savchenkov, and V. S. Ilchenko. “Ultimate Q of optical microsphere resonators.” Optics letters 21.7: 453-455 (1996).

[11] H. Lee, T. Chen, J. Li, K. Y. Yang, S. Jeon, O. Painter, and K. J. Vahala. “Chemically etched ultrahigh-Q wedge-resonator on a silicon chip.” Nature Photonics, 6(6), 369-373 (2012).

[12] A. A. Savchenkov, A. B. Matsko, V. S. Ilchenko, and L.Maleki. “Optical resonators with ten million finesse.” Optics express 15.11: 6768-6773 (2007).

[13] A. L. Mikaelian, and A. M. Prokhorov. “V self-focusing media with variable index of refraction.” Progress in Optics. Vol. 17. Elsevier, 279-345 (1980).

[14] V. S. Ilchenko, A. A. Savchenkov, A. B. Matsko, and L. Maleki, “Dispersion compensation in whispering-gallery modes.” JOSA A, 20(1), 157-162 (2003).

[15] D. Zhu, Y. Zhou, X. Yu, P. Shum, and F. Luan. “Radially graded index whispering gallery mode resonator for penetration enhancement.” Optics Express, 20(24), 26285-26291 (2012).

[16] K. Dadashi, H. Kurt, K. Üstün, and R. Esen. “Graded index optical microresonators: analytical and numerical analyses.” JOSA B, 31(9), 2239-2245 (2014).

[17] Z. Najafi, M. Vahedi, and A. Behjat. "The role of refractive index gradient on sensitivity and limit of detection of microdisk sensors." Optics Communications 374: 29-33 (2016).

[18] S. Balac, M. Dauge, Y. Dumeige, P. Féron, and Z. Moitier. “Mathematical analysis of whispering gallery modes in graded index optical micro-disk resonators.” The European Physical Journal D, 74(11), 1-12 (2020).

[19] A. E. Shitikov, I. A. Bilenko, N. M. Kondratiev, V. E. Lobanov, A. Markosyan, and M. L. Gorodetsky. “Billion Q-factor in silicon WGM resonators.” Optica, 5(12), 1525-1528 (2018).

[20] A. A. Savchenkov, V. S. Ilchenko, A. B. Matsko, and L. Maleki, “Kilohertz optical resonances in dielectric crystal cavities”, Physical Review A, vol. 70, no. 5 (2004).

[21] B. E. Little, J.-P. Laine, and H. A. Haus, "Analytic Theory of Coupling from Tapered Fibers and Half-Blocks into Microsphere Resonators," J. Lightwave Technol. 17, 704 (1999).

[22] D. T. Moore. “Gradient-index optics: a review.” Applied Optics, 19(7), 1035-1038 (1980).